Ring Thruster With Magnetic Bearings

L. Matuszewski, K. Falkowski

Technical University of Gdańsk – Faculty of Ocean Engineering
ul. Narutowicza 11/12
Gdańsk, 80-952, Poland
mailto:leszekma@pg.gda.pl

Abstract - In this new design, an electric synchronous motor mover is integrated with a ring propeller in such a way that the motor's stator in the form of electric windings is built into a nozzle shrouding the propeller, and the motor's rotor in the form of permanent neodymium magnets is built into the propeller's ring. The propeller is shaftless, with the ring joining the blades at the tips. The nozzle has radial cavity that accommodates the ring in such a way that the ring inner surface is an extension of the nozzle inner surface, so the nozzle maintains it's optimal geometry. Furthermore, the ring improves the nozzle-propeller hydrodynamic interaction and efficiency by eliminating the leakage losses between moving blades and the nozzle encountered in traditional designs, such as Kort nozzles. The propeller is supported by and able to transmit the thrust via two self-centered, self-aligned, tapered magnetic bearings that keep the propeller in state of levitation. Magnetic bearings, as compared with roller and journal bearings, have significantly higher efficiency and require less maintenance. The taper enables transmission of both, radial and thrust loads. The propeller's ring sides perform as the bearing's journal surface, and the nozzle ring cavity performs as the mating surface.

I. INTRODUCTION

A patent application has been submitted for a new method of conversion of electrical energy into mechanical and vice versa, and transmission of the mechanical energy in a process. A process here could be marine vessel propulsion and steering, hydroelectric power generation, liquid pumping, gas transmission, or any other process dealing with kinetic energy of fluids. At present, each of these processes requires a system consisting of such devices as prime mover, shafting and propeller in case of marine vessel propulsion, a turbine runner, shafting and generator in case of hydroelectric power generation, or prime mover, shafting and impeller in case of liquid and gas transmission. In each case, the new method integrates the system and reduces it to a single device performing the same function. The effect is lower cost to manufacture, install and maintain, lower weight and less space occupied. At the same time, the process efficiency is higher as explained below. Although ring thruster idea is widely known, a conical electromagnetic bearing in this application is unique. It is a step toward maintenance-free, highly reliable and efficient thrusters, for up to multi-megawatt power range applications. The requirement here is that only acid-proof materials be used.

Unique features and operating principles of the method are presented herein as applied in the marine vessel propulsion, yet they are similar in all the processes mentioned. A marine vessel here means any surface ship, submarine, deep-sea vessel or autonomous underwater vehicle. A marine application has been chosen because a working prototype is now being tested by means of originally designed simulator based on the Matlab/ Simulink software.

II. MAGNETIC BEARINGS

Unique, patent-pending conical magnetic bearings are proposed for a water propeller to suspend the rotor (Fig. 1). There are two magnetic bearings (four actuators). The conical magnetic bearing generates two components of electromagnetic force (vertical and horizontal), which control degrees of freedom of rotor. This is the basic difference between classical, cylinder shaped magnetic bearing system and cone shaped magnetic bearing system. The conical magnetic bearing system reduces quantity of electromagnets, power amplifiers, sensors and controllers. At the same time, this magnetic bearing system limits five degrees of freedom. Sixth degree of freedom is limited by an electrical motor which drives the water propeller

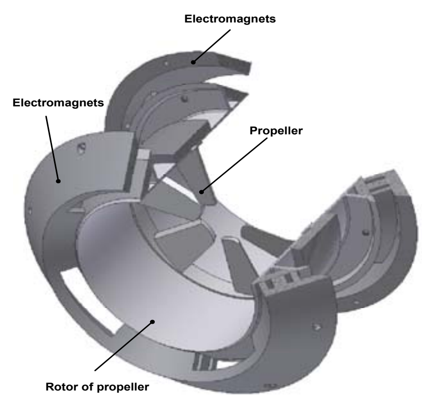

Fig. 1. The conical magnetic bearings.

The rotor of the propeller is in a form of a ring with a large inner diameter (Fig. 2). Blades of the propeller are located inside the ring. On the outside, the rotor is equipped with a race (Fig. 2). The race is a chamfer cone made of ferromagnetic material. It is integral part of the bearing and closes its magnetic circuit. Near the race is a surface which collaborates with eddy current sensors. This surface is made of diamagnetic material. Races and surfaces under sensors are located symmetrically on the rotor (Fig. 2). The armature of electrical motor is located in the central part of rotor.

The rotor is suspended by four homopolar electromagnetic actuators (Fig.3). Electromagnets of the actuators are located in two yokes (left and right – Fig. 1). Each yoke has four electromagnets. Electromagnetic flux is generated by the central magnet lag (Fig. 4). The flux flows through the air gap and race (Fig. 4). It returns through the outside magnet legs (Fig**.** 4). Such a layout of magnet legs reduces to minimum eddy current in the race, because the race moves always under the same legs and the surface of the race does not magnetize. This is typical of homopolar magnetic bearing.

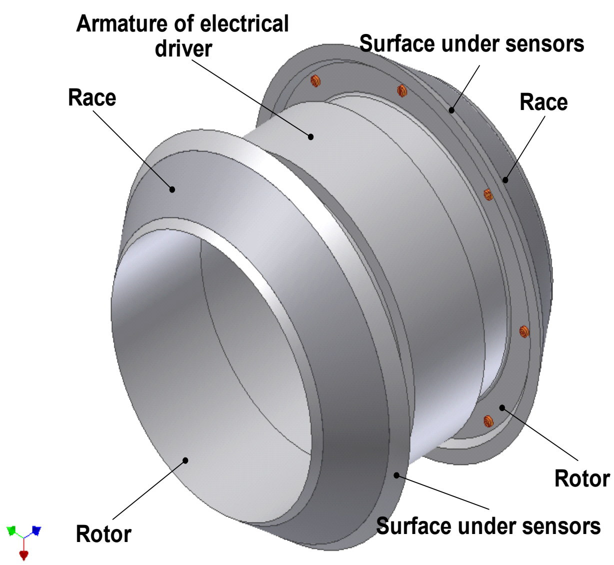

Fig. 2. The rotor of propeller.

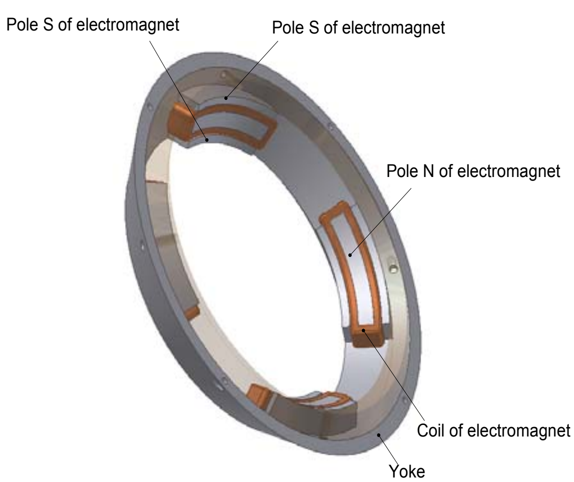

Fig. 3. Yoke with electromagnets

Each differential actuator of magnetic bearing consists of two electromagnets. Electromagnets belonging to one actuator are situated in different yokes (Fig. 5). This is another basic difference between classical magnetic bearing and conical magnetic bearing. In classical magnetic bearing system, electromagnets belonging to one actuator are located in the same yoke.

When the rotor is in point of work (all air gapes are equal) the electromagnets generate similar electromagnetic forces. Resultant electromagnetic force is zero and the rotor does not move (Fig. 5).

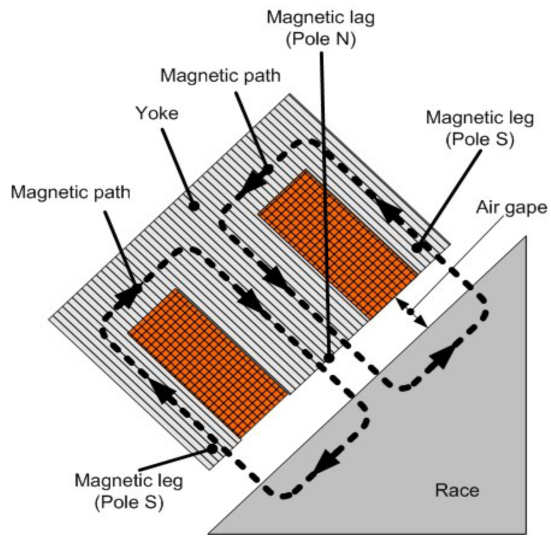

Fig. 4. Elements of magnetic circuit.

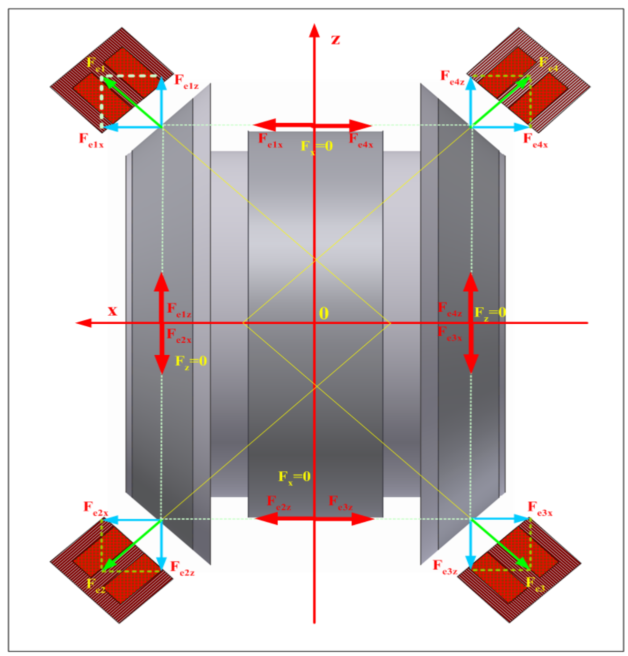

Fig. 5. Rotor of propeller in point of work.

The electromagnetic forces are generated by electromagnets in 0xz plane:

$$
\begin{aligned}
F_{e1x} &= F_{e4x}, \\
F_{e2x} &= F_{e3x}, \\
F_{e1x} &= F_{e2z}, \\
F_{e3z} &= F_{e4z}.
\end{aligned}
\tag{1}
$$

When the rotor moves from the point of work the air gapes will change (Fig. 6). Eddy current sensors measure the movement. A controller uses the sensors information to derive appropriate control signals. These control signals are amplified by power amplifiers to derive the control currents in the coils, causing magnetic forces to act on the rotor.

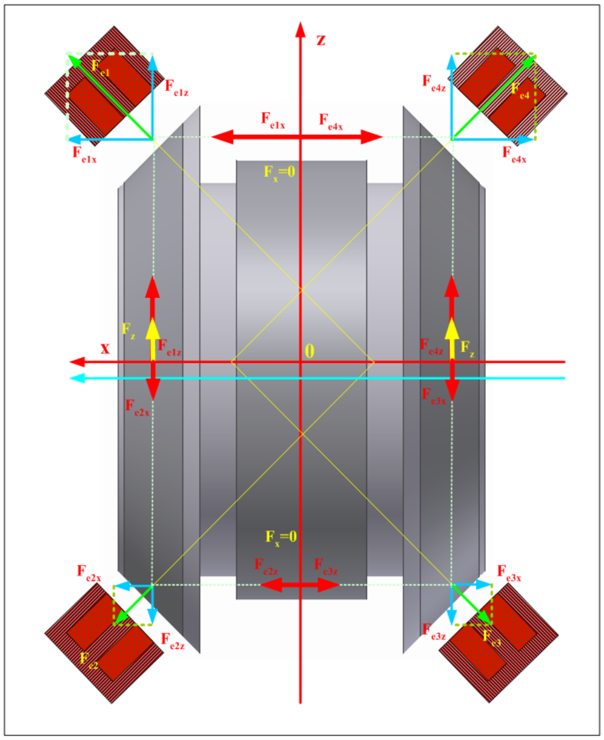

Fig. 6. Rotor of propeller moves down.

When the rotor moves down (direct axis 0z), the sensor produces a displacement signal which leads to increase electromagnetic forces F_{e1} and F_{e4}, but decrease electromagnetic forces F_{e2} and F_{e3}. When components of electromagnetic forces F_{e1z}, F_{e1x}, F_{e4z} and F_{e4x} are increased, the components of electromagnetic forces F_{e2z}, F_{e2x}, F_{e3z} and F_{e3x} are decreased. Between electromagnetic forces lead resultant electromagnetic forces (Fig. 6):

$$
\begin{aligned}
F_{e1x} - F_{e4x} &= 0, \\
F_{e2x} - F_{e3x} &= 0, \\
F_{e1z} - F_{e2z} &\neq 0, \\
F_{e4z} - F_{e3z} &\neq 0.
\end{aligned} \tag{2}
$$

The resultant electromagnetic forces counteract movement of rotor and the rotor returns to the point of work. If the rotor moves in direction of axis Ox, electromagnets increase electromagnetic force F_{e1} and F_{e2} but forces F_{e3} and F_{e4} decrease (Fig. 7). So, components of electromagnetic forces F_{e1z}, F_{e1x}, F_{e2z} and F_{e2x} are increased, the components of electromagnetic forces F_{e2z}, F_{e2x}, F_{e3z} and F_{e3x} are decreased (fig. 7). The resultant of electromagnetic forces is:

$$
\begin{aligned}
F_{e1x} - F_{e4x} &\neq 0, \\
F_{e2x} - F_{e3x} &\neq 0, \\
F_{e1z} - F_{e2z} &= 0, \\
F_{e4z} - F_{e3z} &= 0.
\end{aligned} \tag{3}
$$

The resultant electromagnetic forces counteract movement of rotor and the rotor returns to the point of work.

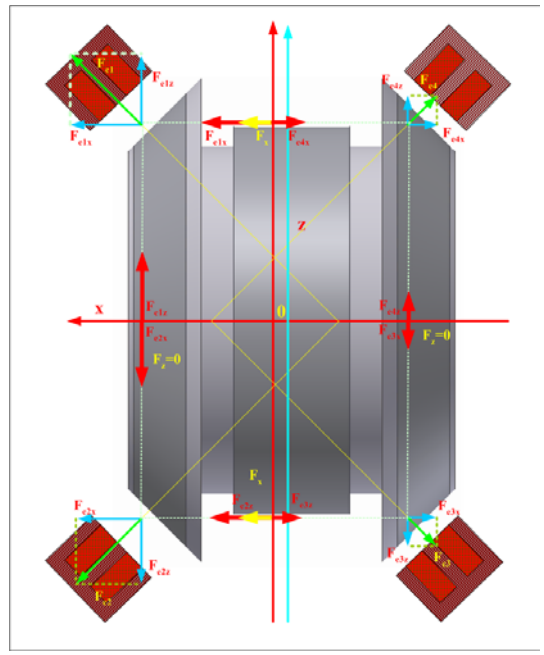

Fig. 7. Rotor of propeller moves right.

Each electromagnet generates electromagnetic forces:

$$
\begin{aligned}
F_{e1} &= k_i i_{w1} + k_s w_1 + F_0, & F_{e3} &= -k_i i_{w1} - k_s w_1 + F_0, \\
F_{e2} &= k_i i_{w2} + k_s w_2 + F_0, & F_{e4} &= -k_i i_{w2} - k_s w_2 + F_0, \\
F_{e5} &= k_i i_{w3} + k_s w_4 + F_0, & F_{e7} &= -k_i i_{w3} - k_s w_3 + F_0, \\
F_{e6} &= k_i i_{w4} + k_s w_4 + F_0, & F_{e8} &= -k_i i_{w4} - k_s w_4 + F_0,
\end{aligned} \tag{4}
$$

where:
k_i – current stiffness,
k_s – displacement stiffness,
i_{w1}, i_{w2}, i_{w3}, i_{w4} – control current,
w_1, w_2, w_3, w_4 – displacement of the rotor in air gaps (this parameters is measured by eddy current sensors),
F_0 – electromagnetic force generated in point of work:

$$
F_0 = \frac{K}{4}\left(\frac{i_0}{x_0}\right)^2
$$

Electromagnetic forces can be collected in vector. It is equal:

$$\mathbf{F_e} = \mathbf{K_i}\mathbf{i} + \mathbf{K_s}\mathbf{w} + \mathbf{F_0}\,, \tag{5}$$

where:

$\mathbf{F_e} = \begin{bmatrix} F_{e1} & F_{e2} & F_{e3} & F_{e4} & F_{e5} & F_{e6} & F_{e7} & F_{e8} \end{bmatrix}^T$ - vector of electromagnetic force,

$\mathbf{K_i} = \begin{bmatrix} k_i & 0 & 0 & 0 \\ 0 & k_i & 0 & 0 \\ -k_i & 0 & 0 & 0 \\ 0 & -k_i & 0 & 0 \\ 0 & 0 & k_i & 0 \\ 0 & 0 & 0 & k_i \\ 0 & 0 & -k_i & 0 \\ 0 & 0 & 0 & -k_i \end{bmatrix}$ - matrix of current stiffness,

$\mathbf{K}_s = \begin{bmatrix} k_s & 0 & 0 & 0 \\ 0 & k_s & 0 & 0 \\ -k_s & 0 & 0 & 0 \\ 0 & -k_s & 0 & 0 \\ 0 & 0 & k_s & 0 \\ 0 & 0 & 0 & k_s \\ 0 & 0 & -k_s & 0 \\ 0 & 0 & 0 & -k_s \end{bmatrix}$ - matrix of displacement stiffness,

$\mathbf{F_0} = \begin{bmatrix} F_0 & F_0 & F_0 & F_0 & F_0 & F_0 & F_0 & F_0 \end{bmatrix}^T$ - vector of forces generated when the rotor is situated in point of work,

$\mathbf{w} = \begin{bmatrix} w_1 & w_2 & w_3 & w_4 \end{bmatrix}^T$ - position vector (elements of vectors are measured by eddy current sensors),

$\mathbf{i} = \begin{bmatrix} i_{w1} & i_{w2} & i_{w3} & i_{w4} \end{bmatrix}^T$ - vector of control current.

Position of rotor is described by two vectors: global position vector and position vector. The rotor position vector is described by five parameters:

x – displacement in the direction axis Ox,
y – displacement in the direction axis Oy
z – displacement in the direction axis Oz,
α – revolution around axis Oy,
β – revolution around axis Oz.

Parameters can be put together in the global position vector (Fig. 8):

$$\mathbf{q} = \begin{bmatrix} x & y & z & \alpha & \beta \end{bmatrix}^T \tag{6}$$

Position vector can be described by global position vector:

$$\begin{aligned} w_1 &= x\sin\gamma + z\cos\gamma + \left(l_z\sin\gamma - l_x\cos\gamma\right)\alpha, \\ w_2 &= x\sin\gamma - z\cos\gamma + \left(l_z\sin\gamma + l_x\cos\gamma\right)\alpha, \\ w_3 &= x\sin\gamma - y\cos\gamma - \left(l_y\sin\gamma + l_x\cos\gamma\right)\beta, \\ w_4 &= x\sin\gamma + y\cos\gamma - \left(l_y\sin\gamma - l_x\cos\gamma\right)\beta. \end{aligned} \tag{7}$$

This relation between vectors is described by equation:

$$\mathbf{w} = \mathbf{T_q}\mathbf{q}\,, \tag{8}$$

where: T_q – transformation of matrix between position vector and global position vector:

$$\mathbf{T_q} = \begin{bmatrix} \sin\gamma & 0 & \cos\gamma & l_z\sin\gamma - l_x\cos\gamma & 0 \\ \sin\gamma & 0 & -\cos\gamma & l_z\sin\gamma + l_x\cos\gamma & 0 \\ \sin\gamma & -\cos\gamma & 0 & 0 & -l_y\sin\gamma - l_x\cos\gamma \\ \sin\gamma & \cos\gamma & 0 & 0 & -l_y\sin\gamma + l_x\cos\gamma \end{bmatrix} \tag{9}$$

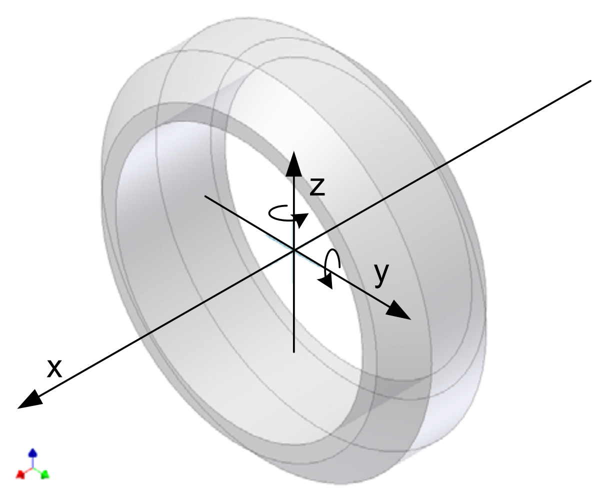

Fig. 8. Global position vector.

Rotor dynamic model:

The rotor of propeller has five degrees of freedom (Fig. 8). It can be described by five differential equations:

$$\begin{aligned}
&m\ddot{x} = F_{ex} + G_x, \\
&m\ddot{y} = F_{ey} + G_y, \\
&m\ddot{z} = F_{ez} + G_z, \\
&I_y\ddot{\alpha} + \left(I_x - I_z\right)\Omega\dot{\beta} = M_{ey} + M_{zy}, \\
&I_z\ddot{\beta} - \left(I_x - I_y\right)\Omega\dot{\alpha} = M_{ez} + M_{zz},
\end{aligned} \tag{10}$$

where:

m – mass of rotor,

I_x, I_y, I_z – axial and radial inertial moments of rotor,

F_{ex}, F_{ey}, F_{ez} –electromagnetic forces generated by electromagnets,

M_{ey}, M_{ez} – moments of electromagnetic force,

G_x, G_y, G_z – external forces which unbalance the rotor,

M_{zy}, M_{zz} –moments of external forces which unbalance the rotor.

Electromagnetic forces are generated by electromagnets:

$$\begin{aligned}
&F_{ex} = \left(F_{e1} - F_{e3}\right)\sin\gamma + \left(F_{e2} - F_{e4}\right)\sin\gamma + \left(F_{e5} - F_{e7}\right)\sin\gamma + \left(F_{e6} - F_{e8}\right)\sin\gamma, \\
&F_{ey} = \left(-F_{e5} + F_{e7}\right)\cos\gamma + \left(F_{e6} - F_{e8}\right)\cos\gamma, \\
&F_{ez} = \left(F_{e1} - F_{e3}\right)\cos\gamma + \left(-F_{e2} + F_{e4}\right)\cos\gamma.
\end{aligned} \tag{11}$$

Equation (4) can be inserted into equation(11):

$$\begin{aligned}
&F_{ex} = \left(F_{w1} + F_{w2} + F_{w3} + F_{w4}\right)\sin\gamma, \\
&F_{ey} = \left(-F_{w3} + F_{w4}\right)\cos\gamma, \\
&F_{ez} = \left(F_{w1} - F_{w2}\right)\cos\gamma.
\end{aligned} \tag{12}$$

where:

$$\begin{aligned}
&F_{w1} = 2k_i i_{w1} + 2k_s w_1, \\
&F_{w2} = 2k_i i_{w2} + 2k_s w_2, \\
&F_{w3} = 2k_i i_{w3} + 2k_s w_3, \\
&F_{w4} = 2k_i i_{w4} + 2k_s w_4.
\end{aligned}$$

Moments of electromagnetic forces are:

$$\begin{aligned}
&M_{ey} = F_1\sin\gamma l_z + F_2\cos\gamma l_x + F_3\sin\gamma l_z + F_4\cos\gamma l_x \\
&-F_1\cos\gamma l_x - F_2\sin\gamma l_z - F_3\cos\gamma l_x - F_4\sin\gamma l_z, \\
&M_{ez} = F_5\sin\gamma l_y + F_6\cos\gamma l_x + F_7\sin\gamma l_y + F_8\cos\gamma l_x \\
&-F_5\cos\gamma l_x - F_6\sin\gamma l_y - F_7\cos\gamma l_x - F_8\sin\gamma l_y.
\end{aligned} \tag{13}$$

If l_x, l_y, l_z distances and γ angle make a good match, moments of electromagnetic forces are zero. System of equations is replaced by matrix equation:

$$\mathbf{M}\,\ddot{\mathbf{q}} + \mathbf{G}\,\dot{\mathbf{q}} = \mathbf{F_e} + \mathbf{F_z}, \tag{14}$$

where:

M – matrix of mass:

G – matrix of gyroscope effect:

$\mathbf{F_e}$ – matrix of electromagnetic moments and forces:

$$\mathbf{F_e} = \begin{bmatrix} F_{ex} & F_{ey} & F_{ez} & M_{ey} & M_{ez} \end{bmatrix}^T$$

$\mathbf{F_z}$ – matrix of external moments and forces

$$\mathbf{F}_z = \begin{bmatrix} G_x & G_y & G_z & M_{zy} & M_{zz} \end{bmatrix}^T$$

$\dot{\mathbf{q}}, \ddot{\mathbf{q}}$ - first and second derivatives of the global position vector **q**:

$$\mathbf{q} = \begin{bmatrix} x & y & z & \alpha & \beta \end{bmatrix}^T$$

If we insert equation (5) in equation (14) we will get:

$$\mathbf{M}\ddot{\mathbf{q}} + \mathbf{G}\dot{\mathbf{q}} = \mathbf{T_F}\left[\mathbf{K_i i_w} + \mathbf{K_s w} + \mathbf{F_0}\right] + \mathbf{F_z}, \tag{15}$$

where:

$\mathbf{T_F}$ – transformation matrix which described relation between electromagnetic forces generated by electromagnets and electromagnetic forces and moments in coordinates of rotor.
In the matrix equation there are two variables, which describe the position of rotor. First variable is global position vector **p** and second variable is position vector **w**. If we take into consideration transformation matrix $\mathbf{T_q}$ between **w** and **q** vectors we will eliminate position vector w from matrix equation:

$$\mathbf{M}\ddot{\mathbf{q}} + \mathbf{G}\dot{\mathbf{q}} = \mathbf{T_F}\left[\mathbf{K_i i_w} + \mathbf{K_s T_q q} + \mathbf{F_0}\right] + \mathbf{F_z}, \tag{16}$$

State space model of water propeller will be assigned from matrix equation:

$$\begin{aligned}\dot{\mathbf{x}} &= \mathbf{Ax} + \mathbf{Bu} + \mathbf{M}^{-1}\mathbf{T}_F\mathbf{F}_0 + \mathbf{M}^{-1}\mathbf{F}_z,\\ \mathbf{y} &= \mathbf{Cx},\end{aligned} \tag{17}$$

where:

A - state matrix:

$$\mathbf{A} = \begin{bmatrix} \mathbf{0}_{5x5} & \mathbf{I}_{5x5} \\ \mathbf{M}^{-1}\mathbf{T}_F\mathbf{K}_s\mathbf{T}_q & \mathbf{-M}^{-1}\mathbf{G} \end{bmatrix}, \tag{18}$$

B - input matrix:

$$\mathbf{B} = \begin{bmatrix} \mathbf{0}_{5x4} \\ \mathbf{M}^{-1}\mathbf{T}_F\mathbf{K}_i \end{bmatrix}, \tag{19}$$

C - output matrix:

$$\mathbf{C} = \begin{bmatrix} \mathbf{T}_q & \mathbf{0}_{4x5} \end{bmatrix}. \tag{20}$$

x – state space vector

$$\mathbf{x} = \begin{bmatrix} \mathbf{q} & \dot{\mathbf{q}} \end{bmatrix}^T, \tag{21}$$

u- control vector:

$$\mathbf{u} = \mathbf{i}_w, \tag{22}$$

y – output vector:

$$\mathbf{y} = \mathbf{w}. \tag{23}$$

The rotor of propeller as open system is unstable. There is controller, which realizes control low:

$$\mathbf{i}_w = \mathbf{-K}_R\mathbf{y}, \tag{24}$$

where: $\mathbf{K}_{Rr}$ – matrix of controller.

If we put output equation in equation(24), we will have:

$$\mathbf{i}_w = \mathbf{-K}_R\mathbf{Cx}. \tag{25}$$

The state space model of the water propeller will change:

$$\begin{aligned}\dot{\mathbf{x}} &= \left[\mathbf{A} - \mathbf{BK}_R\mathbf{C}\right]\mathbf{x} + \mathbf{M}^{-1}\mathbf{T}_F\mathbf{F}_0 + \mathbf{M}^{-1}\mathbf{F}_z,\\ \mathbf{y} &= \mathbf{Cx}.\end{aligned} \tag{26}$$

Geometric analysis allows to estimate the race overall surface as A=1269.72 [mm^2], and enables to gain magnetic induction of 1.5 [T], hence maximum force generated is Fmax = 2272 [N]. Table 1 shows the force changes vs. magnetic induction variable from 0.9 up to 2 [T] for a single electromagnet with air gap 0.3mm.

Table1 Force generated vs. material properties

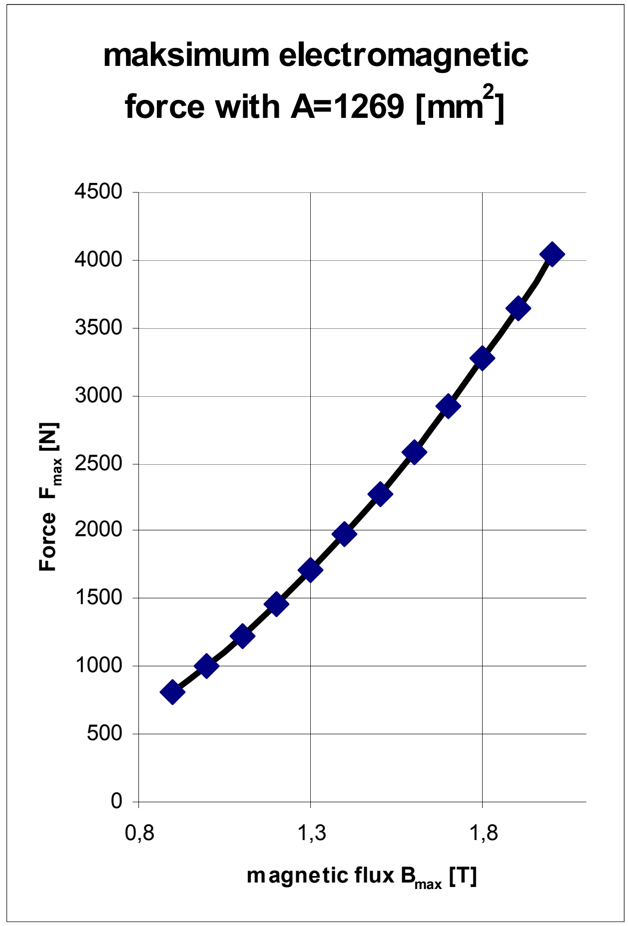

III. OVERVIEW OF THE PROPELLER PROTOTYPE PROPERTIES

Ring propeller modeling is quite new task and there is insufficient experimental data to verify analytical method calculation for design and therefore for later optimization, too. Most significant properties are absence of shaft and no gap between the end of blade and the nozzle when compared with traditional propeller in Kort nozzle. It is therefore important for the propeller designer to have a method for the analysis of intrinsic phenomena, in order to keep them under control from the very beginning of the design procedure. Such a method should definitely enable calculation of the fluctuating bearing forces coming up also from unsteady cavitation phenomena including time - dependent volume of cavities and resulting pressure pulses inducted in the surrounding space. When traditional bearings are used the forces could damage them, but significant advantage of magnetic bearings allows to reduce the forces and vibrations almost to zero. A bearing stability problem still remains for controller if mentioned forces gain critical level. In this way, the unsteady cavitation regarded as a continuous affects bearing present situation. The theoretical model of the propeller is based on the discrete gridwork of vortex elements simulating the loading distribution and the discrete gridwork of sources simulating the finite thickness of the blade. The structure of the model is schematically presented in the Fig. 9. The computational model is based on the discrete mesh of the vortex and source singularities. On each blade 165 elements of the bound vortices **B** are placed which model the hydrodynamic load distribution on the lifting surface (Fig 9). Each of the elements represent the vorticity concentrated on the surface **ΔS**. To be in compliance with the Kelvin principle on the vorticity conservation, the bound vortices should be supplemented by the set of 168 elements of the bound vortices **T**. The intensity of **T-**elements can be expressed by a linear combination of the intensities of **B-**elements located on the lifting surface strips neighboring on each other.

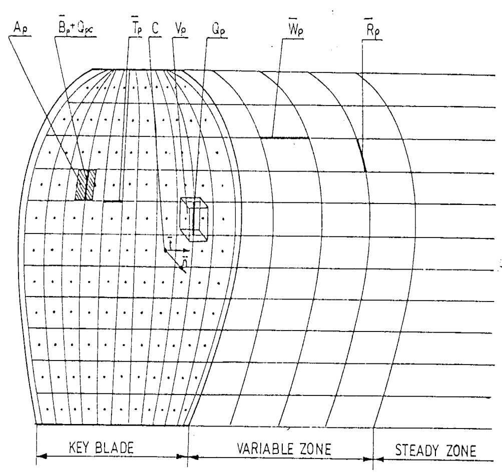

Fig 9. Discrete vortex/source model of the propeller blade

Behind the blade trailing edge the helix surfaces are formed from the elements of the free vortices **W** which are extensions of the trailing vortices **T**. The part of the free vortex system, closest to the trailing edge, forms the variable zone of the free vortex system in which the radius –oriented vortex elements **R** exist additionally. The remaining part of the system forms the steady zone consisting of the elements **W** only. The variable zone influences, by the induced velocities, an actual kinetic situation on the blade. The blade thickness as well as the sheet cavity thickness is modeled by means of the sources and sinks discrete distribution **q**. The classical linearization assumption is applied dealing with the separation of the hydrodynamic loading effect from the thickness effect. The key point of the method is the kinematic boundary condition on the lifting surface which requires the resultant relative velocity of flow to be tangent to the surface. It leads to the following integral equation:

$$\frac{1}{4\pi}\left[\iint_{S_c}\vec{n}\gamma\nabla\left(-\frac{1}{r_p}\right)dS+\iint_{S_p}q\frac{\partial}{\partial n}\left(-\frac{1}{r_p}\right)dS\right]+\left(\vec{V}+\vec{\omega}\times\vec{r}\right)\cdot\vec{n}=0 \qquad (27)$$

where:

$$\gamma = \gamma_p + \gamma_{pv}$$

$$q = q_p + q_c$$

n-vector normal to the surface, γ-vortex element intensity, V-flow velocity inducted, Sc-area of the vortex surface, r_p-distance between the control point and vortex element , Sp-propeller blade area, q-source intensity, Vo-hull speed, ω-angular velocity, r-radius vector, q_p-source intensity modeling the blade thickness, q_c- source intensity modeling the cavities, γ_p-vortex element intensity on the lifting surface, γ_{pv}-vortex element intensity of the free vortex system.

By solving the equation numerically a set of linear equations is obtained, however in order to complete the system the Kutta condition on the trailing edge is used additionally. The linear equation system is solved by applying the Gauss-Jordan elimination method with the basic element selection. When the intensities of the vortex elements **B, T, W** and **R** are already determined it is possible to determine the induced velocities on the lifting surface, as well as those at an arbitrary point of space surrounding the propeller. The Biot-Savart expression is applied to calculate the induced velocities. A number of bound vortex elements is located on the surface defined by the mean lines of all blade section. Typically the spacing of bound vortices is more dense in the area close to blade trailing edge. This is done in order to model properly more abrupt changes in loading distribution expected in the vicinity of the leading edge and to enable more precise analysis of the initial stages of the sheet cavity development. The elementary line sources coincide with the bound vortex elements. One of the propeller blades is distinguished as the key blade. A set control points is located in this blade, placed exactly in the middle of quadrangles formed by the adjacent bound and trailing vortex elements. The intensity of the bound vortex elements closest to the blade trailing edge is related to the intensity of the proceeding elements on the basis of Kutta-Joukovski condition, thus reducing the number of vortex elements of unknown intensity to the number of control points. Standard configuration consists of 11 chordwise strips with 15 control points in each of them. Free vortex surfaces extend behind all blades. These surfaces are built of the free vortex lines of regular helical shape. Pitch of the free vortex lines is calculated as a linear combination of the mean blade pitch and the mean inflow inclination. Only the surface behind the key blade has the so-called variable zone, located immediately behind the blade trailing edge. This zone reflects the changing flow conditions on the key blade and the sections of the same free vortex line may have different intensities there. This possibility results in the presence of radial vortex elements, in order to fulfill the requirements of the circulation conservation theorem. Apart from that, the set of control points is placed in the variable zone in anticipation of sheet cavities extending beyond the trailing edge of the blade. The geometry of the whole vortex model of the propeller is not affected by the circumferential non-uniformity of the inflow velocity field. Similarly, the intensities of bound and trailing vortices on all blades except the key blade and intensities of the free vortices and sources simulating the blade thickness are regarded as being constant with time. These intensities result from the circumferentially average inflow velocity field. Only the distributions of vorticity on the key blade and in the variable zone follow the circumferential non-uniformity of the inflow velocity field. The unknown intensities of the bound vortex elements may be obtained from the kinematic boundary condition on the lifting surface of the key blade. This condition requires that the vector of the resultant flow velocity including induced velocities should be tangential to the lifting surface. Evaluation of this condition leads to the system of linear equations for the intensities of the bound vortex elements , each equation corresponding to one control point on the key blade. The Biot-Savart formula is employed for the calculation of the velocity induced by the vortex elements of the lifting surface model. Once the system of linear equations is solved , the resulting tangential induced velocities may be calculated. Then the pressure distribution on the key blade may be obtained from the following Bernoulli formula

$$C_p = \frac{p - p_\infty}{\frac{1}{2}\rho V_0^2} = 1 - \left(\frac{V_p}{V_0}\right)^2 - \frac{2}{V_0^2}\frac{\partial \Phi_S}{\partial t} \qquad (x)$$

where: Cp - non-dimensional pressure coefficient, p – pressure at the point of question, $p\infty$ - pressure at infinity, ρ - density of water, $V\infty$ - flow velocity at infinity, Vi – resultant flow velocity at the point of question, φ - velocity potential reflecting the loading distribution on the key blade.

Propeller Prototype Data:

Inner ring diameter	D=0.20 m
Available maximum torque	Q=50.0 Nm
Speed in water	V_1=1.0 m/s
With propeller velocity	n_1=3000 rpm
Speed in water	V_2=0.0 m/s
With propeller velocity	n_2 =2500 rpm
Ring width at blade fixed point	c=0.06 m.

Reversible thruster should have symetric blades profile toward all two axis, and to incr付rse efficiency ellipsoid shape had been chosen. For preliminary calculations V_2=0 m/s and velocity n_2=2500.0 1/min had been taken due to practical reasons. A number of blades in prototype considered among Z=4, 5 and 6 when ellipsoid shape taken. Results of analysis shown at Tab 2

Tab 2 Propeller's coefficients vs. blades quantity

Z	4	5	6
P/D	1.385	1.335	1.300
$(C/D)_{1.0}$	0.4922	0.3938	0.3282
K_T	0.3963	0.4102	0.4226
K_Q	0.09196	0.09180	0.0921

Where:

P/D-pitch coefficient,
$(C/D)_{1.0}$-relative end of blade width
$K_T=T/\rho n^2D^4$ - thrust coefficient
$K_Q=Q/\rho n^2D^5$ - torque coefficient

Practically, for the same K_Q (with the same power transmitted by the propeller) the quantity of blades increasing results of higher thrust coefficient – thus quantity of Z=6 seems optimal at the particular case. So, for 6 blades prepared the thruster ring where all blades welded in and fixed to the whole device.
For P/D = 1.26 = const, results K_T = 0.442 and K_Q = 0.0903 when propeller's velocity n = 2500 rpm and propeller axis level is h = 2.5 m beneath the water surface laminar cavity is encountered for r/R >= 0.6. For radius r/R = 0.9 cavity surrounds nearby 35% of blade length. Profiles coordinates shown on Table 2

Table 2. Blade length and maximum thickness

r/R	C [mm]	t_{max} [mm]
0.2	3.0	1.0
0.3	32.0	1.8
0.4	45.0	2.4
0.5	50.0	3.0
0.6	53.0	3.6
0.7	56.0	4.2
0.8	59.0	4.8
0.9	62.0	5.4
1.0	65.0	6.0

The trials of the ring thruster prototype are underway. Special magnetic bearings simulator has been constructed for researching high power transmission. Main problem to be resolved successfully is instability avoidance in extreme conditions. Please contact the authors for a copy of the assumptions made to build the prototype, and for the current trial results

IV. REFERENCES

1. Z. Gosiewski, K. Falkowski, "Magnetic Bearing Design For Underwater Robot Drive", Conference on Automation, Innovations and Perspectives – Automation 2003, Warsaw, Poland 2003.

2. Koronowicz T., Szantyr J., Jarzyna H: „Design Theoretical Model For Determination Of The Pressure Field Resulting From Hull Flow And Operation Of The Marine Propeller". Polish Maritime Research, no 3 (13) September 1997 Vol. 4

3. Z. Gosiewski, K. Falkowski, "Multifunctional Magnetic Bearing",Publishing house ITL, Warsaw, 2003r